Biomimatic material(생체 모방 재료)의 크리스탈 공학에 대한 연구동향

Chung-Ang University, Da Vinci College of General Education
OK JA Yoon

CHERIC
Chemical Engineering and Materials Research Information Center
국가지정
화학공학소재연구정보센터

연구 동향

✓ **Bio-inspired photonic crystals for naked eye quantification of nucleic acids[1]**

- 육안 핵산 정량화(naked eye nucleic acid quantification)를 위해 사막 딱정벌레 껍질을 모방한 칩 개발을 보고하고 있으며 자외선 국소 조사에 의해 처리된 소수성 광 결정 기판은 digital loop-mediated isothermal amplification (dLAMP)에 의해 샘플을 수백 방울로 잘 분산시킬 수 있어 마이크로 크기의 광 결정 구조를 조절함.

- LAMP 반응에 의해 만들어진 피로인산 (Pyrophosphate, PPI)은 마그네슘 이온과 결합하여 난용성 침전물 (poorly soluble precipitate)을 형성하였으며 이것은 복합화 형성으로 인해 실리카 기판에 고정되면서 결과적으로 광 결정의 구조적 색이 사라지는 결과를 확인함.

- 구조적으로 색이 없는 점의 수는 샘플에서 핵산 (nucleic acid)을 복사한 수(copy number)에 대한 정보를 포함함으로 이 칩은 형광이나 다른 발색 시약 없이 살모넬라 DNA를 육안으로 검출 할 수 있음을 입증함.

- 새로이 설계된 칩은 제한된 자원 설정 (limited resource settings, LRS) 하에서 디지털 핵산(nucleic acids) 검출 개발을 돕고 POCT (Point of Care Test) 표준에 적합함을 보여줌.

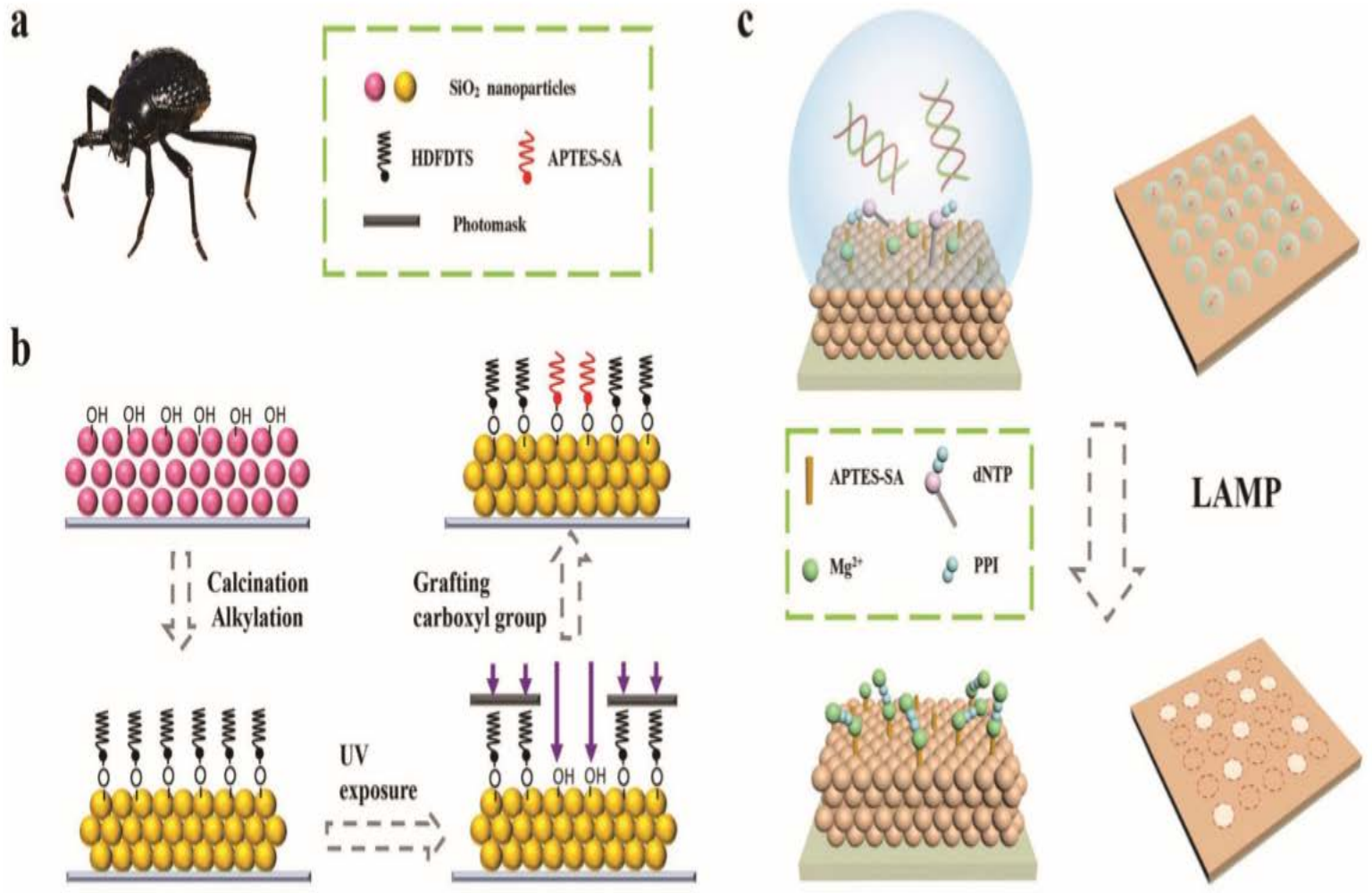

Fig. 1 (a) The photograph of *Stenocara gracilipes*, one of the desert beetles. (b) Schematic of the preparation of hydrophilically patterned photonic crystal substrate. (c) Schematic of the process of LAMP-based quantification and naked eye detection of nucleic acids.

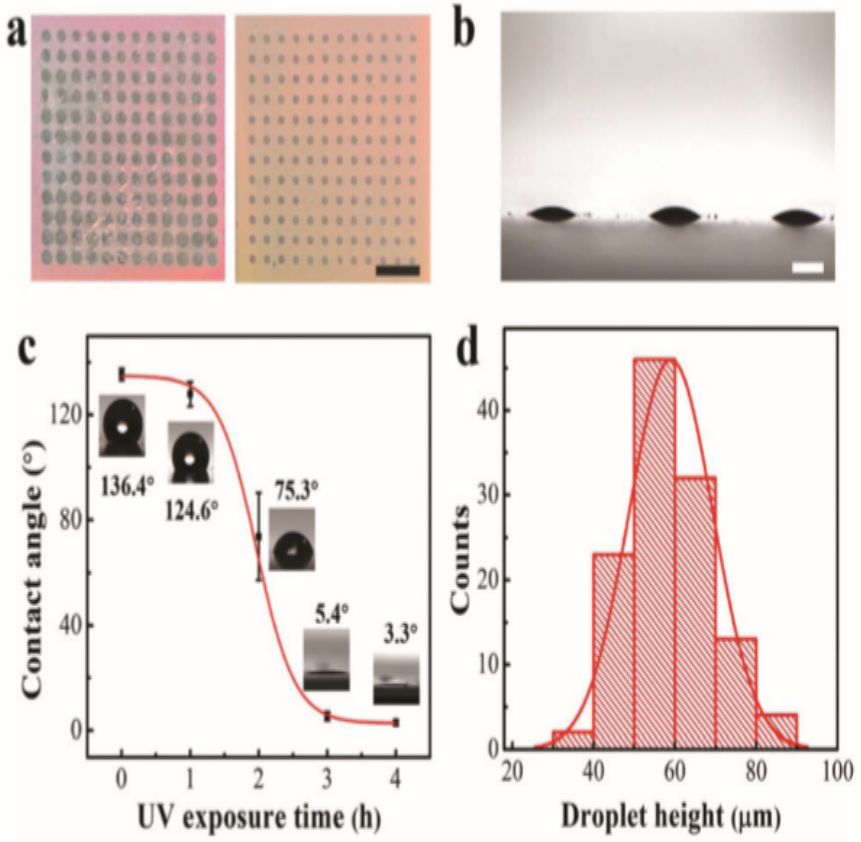

Fig. 2 (a) Comparison of droplet arrays of uncalcined PC substrate (left) and calcined PC substrate (right). Scale bar: 6.0 mm. (b) Photograph of the formed microdroplets on the patterned PC array. The contact angle is indicated as 14.4°. Scale bar: 500 μm. (c) Sample contact angles measured on the UV exposure-treated PC substrate. The test images were captured at 0, 1, 2, 3, and 4 hours. (d) Distribution histogram of the height of all microdroplets formed on the substrate.

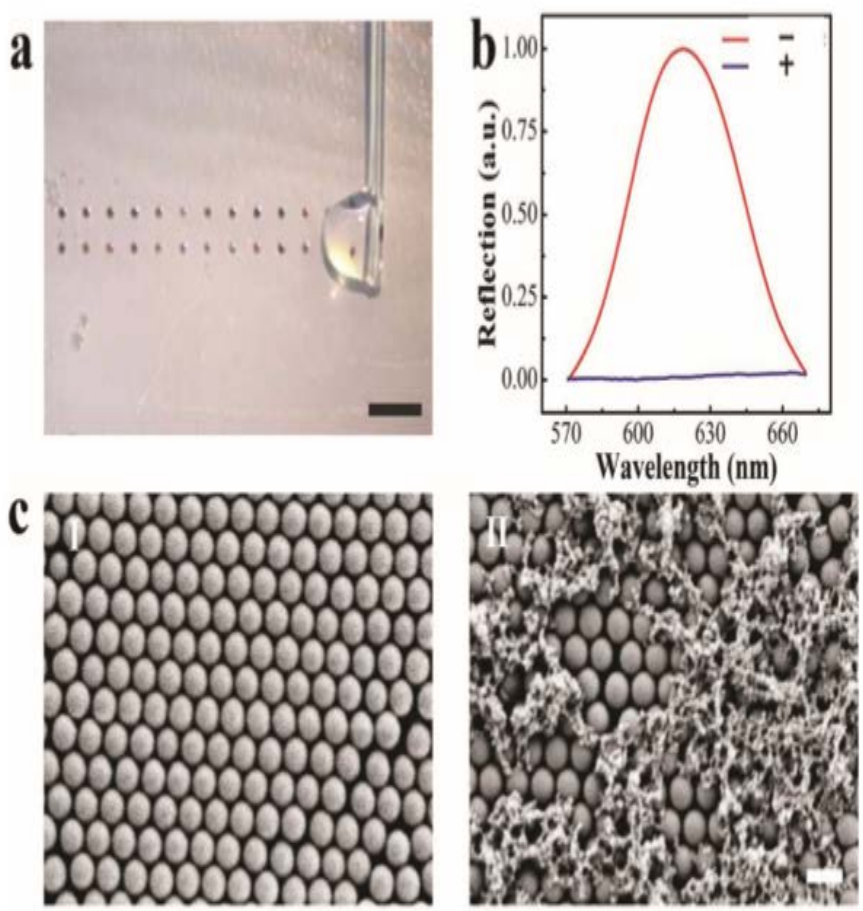

Fig. 3 (a) Photograph of the formation of microdroplets on the PC substrate by a hydrophobic bar. Scale bar: 4.0 mm. (b) The reflection peak spectrum of positive dot (+), negative dot (–). (c) Scanning electron microscopy (SEM) images of the negative dot (I) and positive dot with $Mg_2P_2O_7$ precipitates (II). Scale bar: 400 μm.

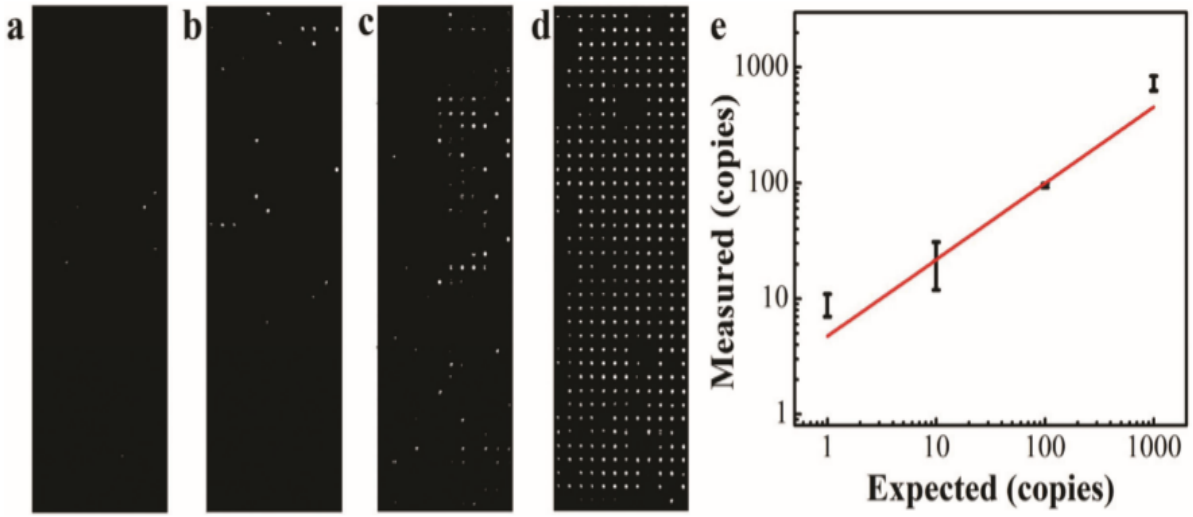

Fig. 4 (a–d) Images of chips with a serial dilution of the target DNA ranging from 1, 10, 100 to 1000 copies per μL after LAMP with image processed. (e) The linear regression curve of copy number between measured and expected copies. The error bars represent standard deviation for three replicated measurements.

Table 1 Comparison of our method and correlative quantification methods of nucleic acids based on LAMP[21,33–35]

Performance	Our method	dLAMP	dLAMP (commercial)	qLAMP
Detection signal	Structural color	Colorimetric dye	Fluorescence	Fluorescence
Dynamic range	4 orders of magnitude	N/A	2–6 orders of magnitude	>9 orders of magnitude
Sensitivity	~7 copies	~8 copies	~5 copies	1–2 copies
Optimized time (min)	60	50	60	60
Partition volume (nL)	16	15	0.004–0.85	N/A
Instrument ($)	UV light ~2k	Lithography machine ~160k	Commercial equipment ~50k–250k	Commercial equipment ~25k–50k
Cost and sample ($)	~1k	N/A	5–400	2

Specifications not available are marked with N/A.

✓ BiomimeticChiral Photonic Crystal[2]

- 딱정벌레 큐티클(외피)의 놀라운 무지개 빛깔의 색상은 바이오 섬유의 복잡한 나노 스케일로 구성되어있음을 잘 알려져 있지만, 비슷한 인공 무기 재료로 광학 반응을 이용해서 만든 비생물적 나노 스케일은 아직 합성되지 못하였음.

- 이 논문은 콜로이드 무기 나노 와이어의 Langmuir-Schaefer assembly에 의한 생체 모방 키랄 광자 결정 (chiral photonic crystals)의 제조 방법을 설명하고 있으며 딱정벌레에서 관찰되는 복잡한 나선형 구조와 원형 편광 반사를 재현했을 뿐만 아니라 키랄 무기 나노 구조에 대한 ~1.6의 dissymmetry factor를 보고함.

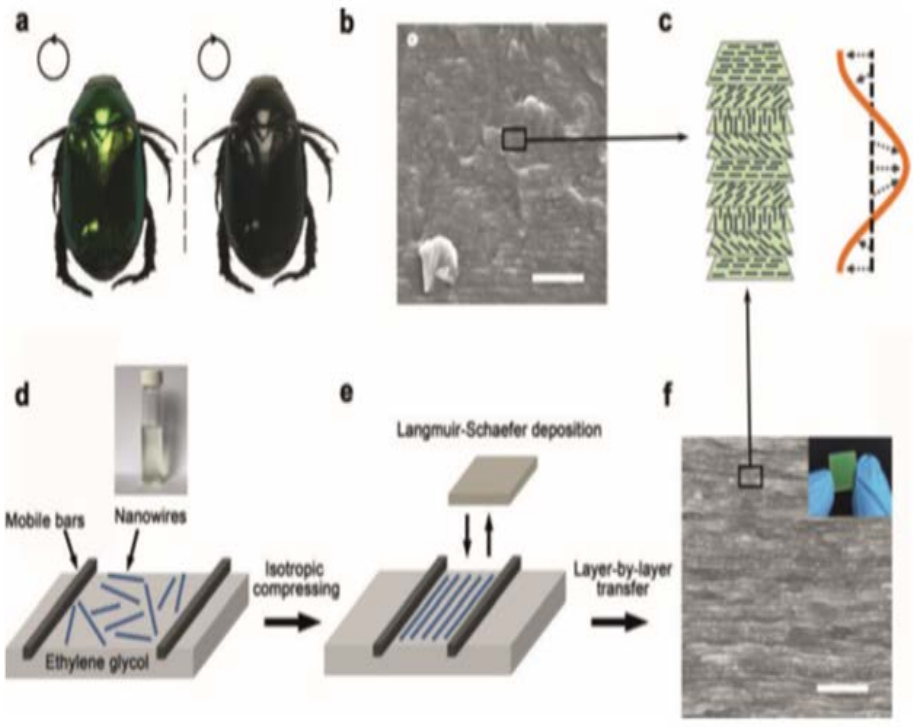

Figure 1. A biomimetic route to chiral photonic crystals. a) Photographs of *Anomala corpulenta* Motschulsky (a scarabaeid beetle) taken through a left- (left photograph) or right-circular (right photograph) polarizer, respectively. b) Scanning electron microscopy (SEM) image of a cross-section of cuticle of *Anomala corpulenta* Motschulsky, showing the layered structure. c) Helical arrangement of aligned layers in the chiral photonic crystals. d) Dispersing nanowires at the air–liquid interface in Langmuir trough; top: photograph of a cyclohexane solution containing $NiMoO_4 \cdot xH_2O$ nanowires. e) Compressing barriers to obtain aligned nanowire films, followed by transferring the aligned layer onto a substrate by horizontal lifting (Langmuir–Schaefer deposition). f) SEM image of the cross-section of a chiral photonic crystal film obtained by layer-by-layer transfer with a predesigned twisting angle; inset: corresponding photograph of the film. Scale bars for (b) and (f): 2 μm.

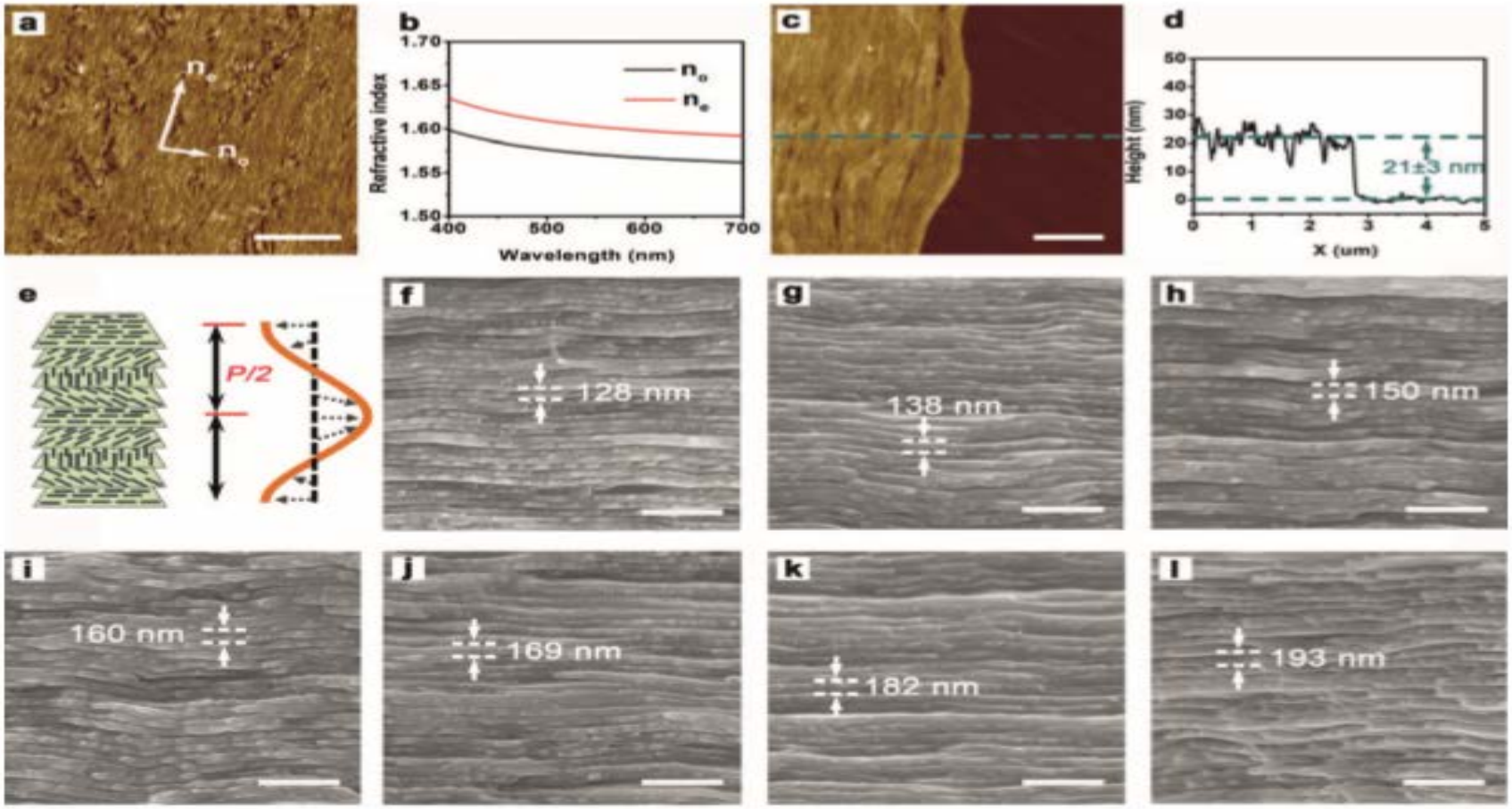

Figure 2. Structures of the biomimetic chiral photonic crystals. a) AFM image of aligned nanowires in one film layer. b) Refractive index of an ordinary ray (n_o) and an extraordinary ray (n_e) shown in (a). c, d) AFM measurement of the thickness of one nanowire film layer. e) Scheme denoting the half pitch of the chiral structure. f–l) SEM sectional images of the chiral photonic crystals. From (f) to (l), each pitch contains 11 to 17 nanowire film layers. Scale bars: 5 μm for (a), 1 μm for (c), and 500 nm for (f)–(l).

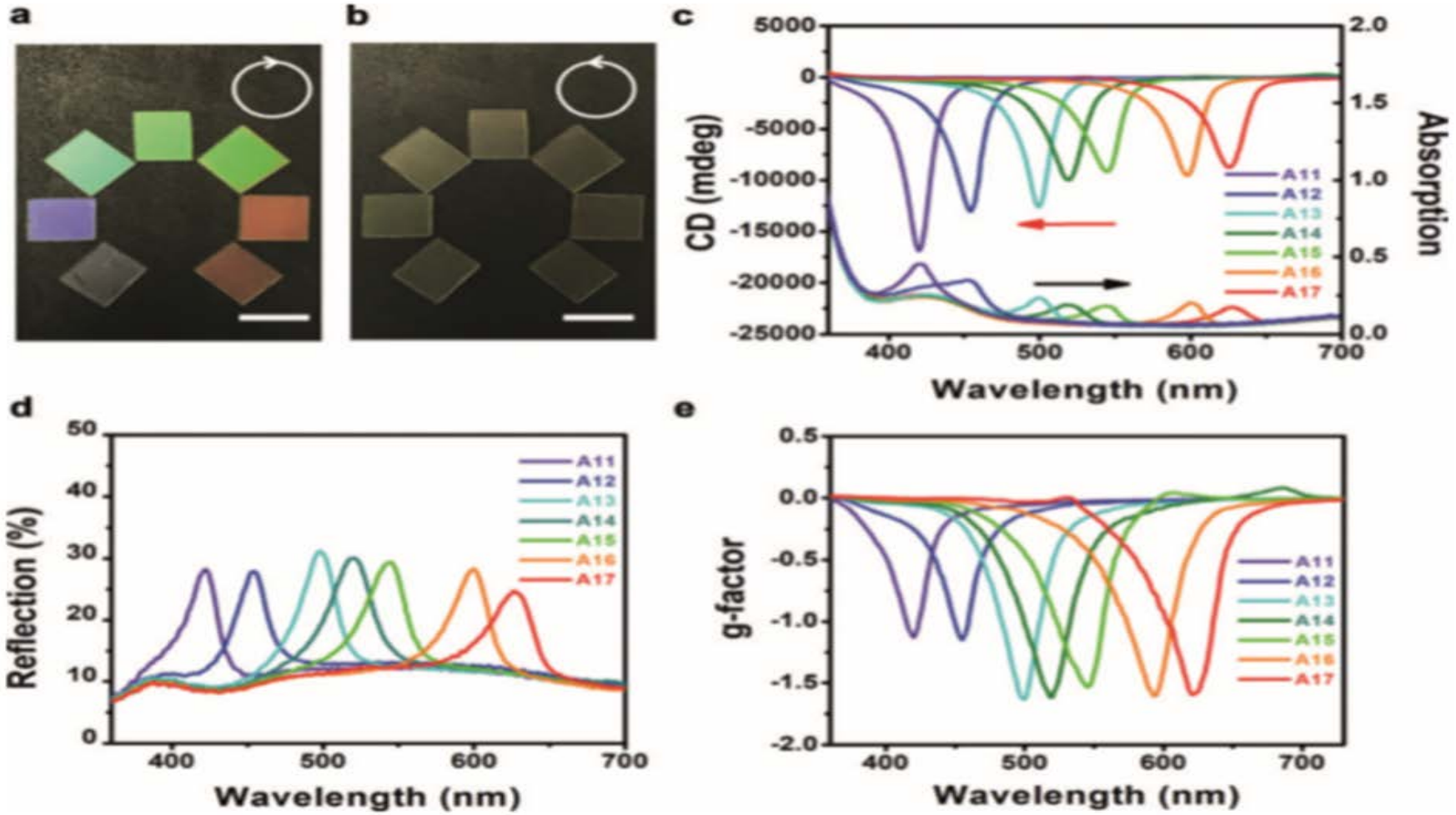

Figure 3. Optical characterization. Chiral photonic crystals viewed through a right- (a) or left- (b) circular polarizer. c) CD and absorption spectra of seven samples. **A11**–**A17** stand for samples with a full pitch containing anticlockwise-rotated 11 to 17 nanowire film layers, respectively. d) Reflection spectra of the samples. e) The *g*-factors of the samples. Scale bars: 1 cm for (a) and (b).

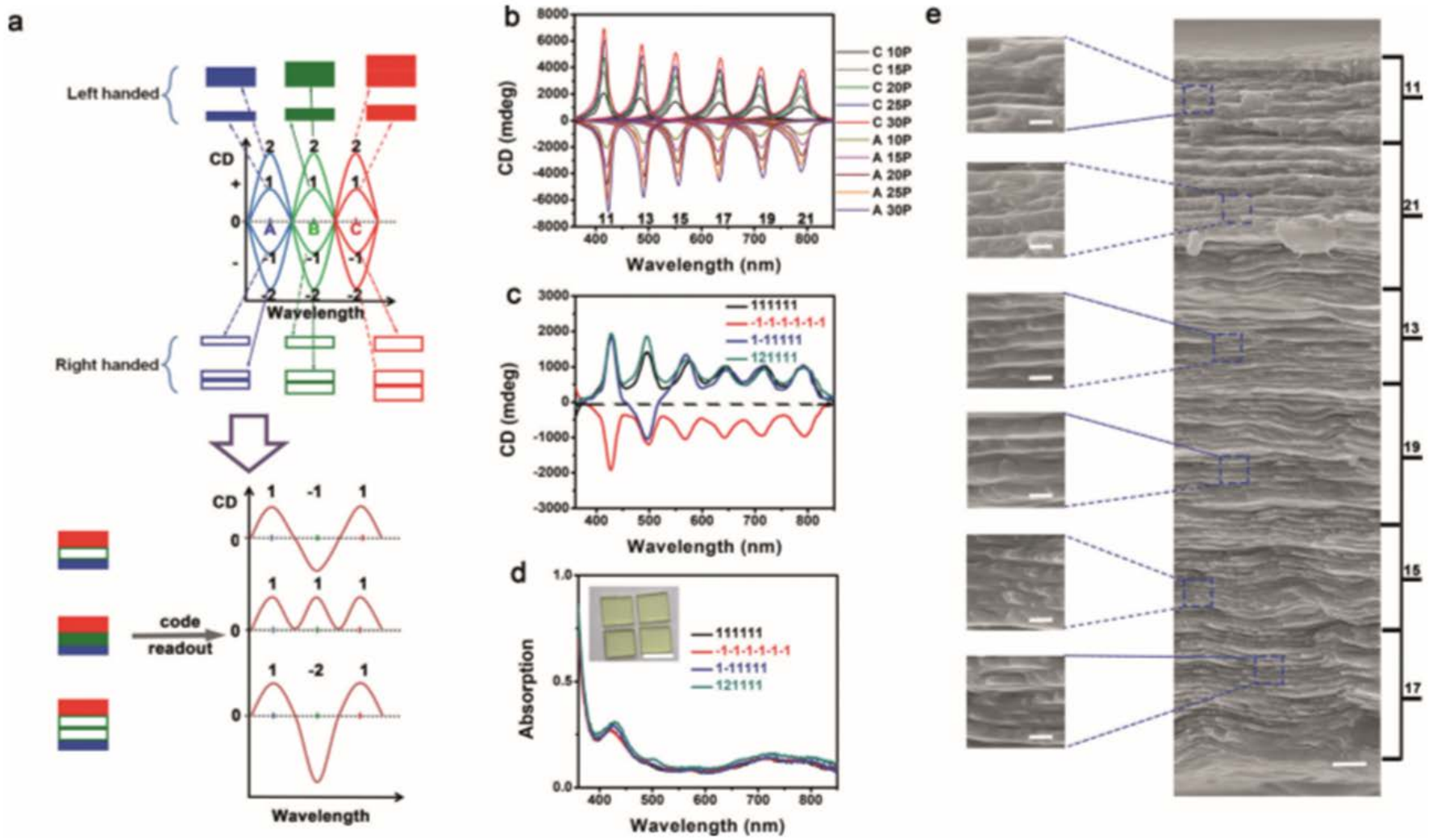

Figure 4. CD spectroscopy coding. a) Coding and readout process. A calibration curve is first established to correlate the structure, CD peak, and digital information (top). Each rectangle represents a certain number of pitches. Afterwards, the codes are built through combinations of the building elements and then read out as digital information by comparing with the calibration curve (bottom panel). b) CD intensity variation with pitch number at six different peak positions. The number above the horizontal axis represents the number of film layers to implement a full pitch, determining the pitch length. For right labels, C 10P stands for the sample containing 10 pitches formed with clockwise transfer, while A 10P denotes the sample formed with anticlockwise transfer. c) CD spectra of four coding samples. Each sample is read out as the digital sequence shown in the corresponding label. d) Absorption spectra corresponding to (c). Inset: Photograph of the four samples taken under natural light. e) SEM cross-sectional images of a coded sample named 111111. The number highlights that the sample contains six regions with CD responses at different wavelengths. Scale bars: 1 cm for (d), 200 nm for the left images in (e), and 1 μm for the right image in (e).

✓ Biomimetic photonics[3]

- 자연에서 영감을 얻은 생체 모방 기술은 광학적 센싱, jamming-avoiding communication links, adaptive visual camouflaging, 수동 온도 조절 미세 구조 (passive temperature regulation), 나노 패턴 표면에 의한 흡수와 효율적인 광 반사 방지, 나노/마이크로 구조 물질부터 선택적 광 산란을 통한 구조적 색상 및 편광 형성을 포함하여 광범위한 응용 분야에 이용되고 있음.

- Dinneen등의 연구는 그림 1 (a)에 표시된 것과 같이 두족류의 크로마토그래피에서 추출한 안료로 구성된 에어로졸의 굴절률을 결정하기 위한 반복적인 보정 방법에 대해 보고하고 있는데 이 안료는 피부 착색에 중요한 역할을 하며, 적용하기 쉬운 스프레이-코팅의 가능성을 제공함.

- Chan 등의 연구는 넓은 범위의 주파수에서 효율적인 반사 방지 특성을 보이는 피치 블랙 표면의 개발에 중점을 두고 있으며 그들이 개발한 반사 방지 구조는 나방의 눈에서 발견되는 복잡한 그래이드의 인덱스 나노 구조 (intricate grade-index nano-structure)에서 영감을 얻었음. (그림 1 (b) 참조).

- Mendoza-Galván 등은 나노 결정질 셀룰로오즈로 만들어진 chiral freestanding films에서 선택적 브래그 반사를 설계함. 선택적 브래그 반사 현상은 일반적으로 딱정벌레 피부의 키랄 구조처럼 비편광 및 입사광을 선택적으로 반사하여 밝은 색을 생성하는 일부 딱정벌레 (그림 1 ©)에서 볼 수 있음. 이러한 원리를 생체 모방하여, 네마틱 키랄 액정상 (nematic chiral liquid crystal phase)에서 수성 셀룰로오즈의 느린 증발을 통해 키랄 구조를 필름에 적용하여 개발함.

- Potyrailo와 동료들은 다변형 광 센서 (multivariable photonic sensors)의 개발에 대해 보고하고 있으며, 그 디자인은 모포 나비(Morpho butterfly) 스케일의 구조에서 영감을 얻어 설계됨. (그림 1 (d)). 연구진은 H_2, CO 및 CO_2와 같은 비응축성 가스 (noncondensable gases)를 탐지하기 위한 가스 센서로 bio-inspired materials를 사용함.

- McDougal과 연구진들의 리뷰는 기능적 특성을 가진 나노 공학 재료를 생산하는 다양한 자연적이나 합성하는 제조 전략을 검토하고 비교했으며 이 포괄적인 연구를 통해 마이크로/나노 스케일 재료의 성능을 보다 잘 이해하여 활용방안과 비용적인 효율성을 검토하는 작업을 거쳐 산업화의 새로운 프로세스 개발을 보고함.

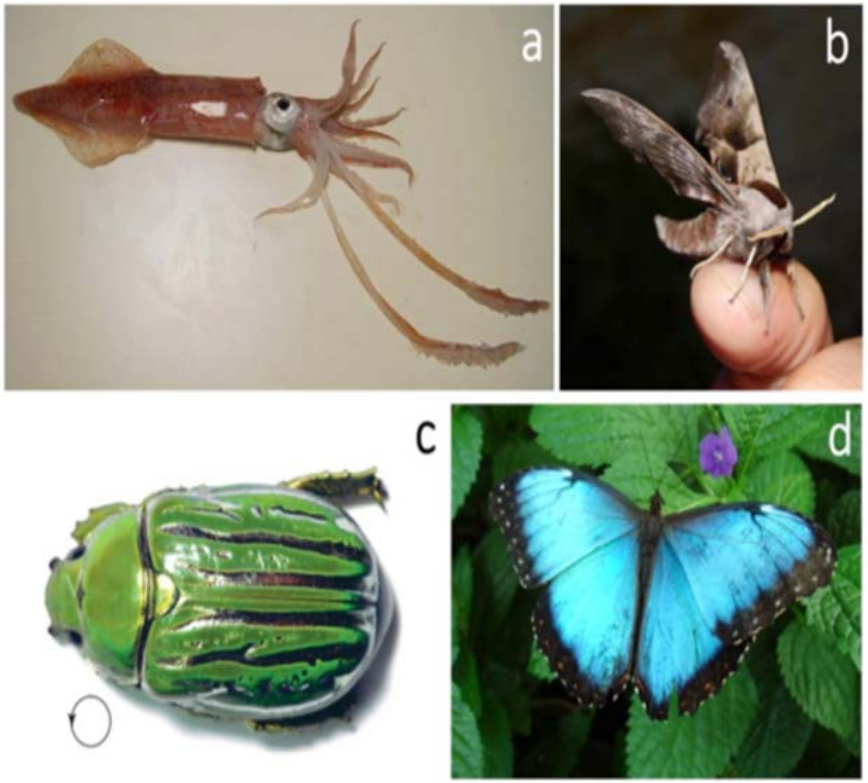

Figure 1. (a) Longfin inshore squid (*Loligo pealeii*), one of many types of squid capable of manipulating their color to vary in color from a deep red to a soft pink. (b) Smerinthus ocellata (*Sphingidae*) (eyed hawk moth), one of many moth species whose eyes' nanoscale gradient index structure allows for efficient anti-reflectance with large field of view and bandwidth. (c) Jewel scarab (*Chrysina gloriosa*) is an example of a beetle specie whose cuticles reflect near circular left-handed polarized light in the visible range. (d) Blue morpho butterfly (*Morpho achilles*) reflects visible light selectively owing to its resonant scattering of the periodic arrangement of micro-scale lamellae, ribs, and ridges within its wings. Image credits: (a) Reproduced from https://commons.wikimedia.org/wiki/File:Loligo_pealeii.jpg. Image stated to be in the public domain. (b) This Smerinthus ocellata (*Sphingidae*) (eyed hawk moth) — (imago), Gent, Belgium' image has been obtained by the author (s) from the Wikimedia website where it was made available by BartBotje under a CC BY 3.0 licence. It is included in this article on that basis. It is attributed to Dimitry De Wilde. (c) Reproduced with permission from [31], © AAAS. (d) This 'Blue Morpho butterfly at Niagara Parks Butterfly Conservatory, 2010 E' image has been obtained by the author(s) from the Wikimedia website where it was made available by Rlevse under a CC BY-SA 3.0 licence. It is included within this article on that basis. It is attributed to Rlevse.

✓ Structural color three-dimensional printing by shrinking photonic crystals[4]

- 일부 나비, Pachyrhynchus weevils, 카멜레온의 착색은 화려한 패턴을 만드는 광 결정에 의한 것으로 알려져 있으며 나노 기술의 발전에도 불구하고, 아직까지 미세한 길이 스케일을 가진 3 차원의 임의의 색상과 모양을 프린트하는 능력이 부족함.

- 이 논문은 격자 상수를 5배 감소시켜 3D 프린팅된 광 결정을 생성하는 열-수축 방법 (heat shrinking method)을 소개하고 있으며 이러한 격자 구조를 3D 컬러 체적 요소로 사용함. 최초로 멀티 컬러 현미경 모델을 이용하여 높이가 39μm, 컬러 픽셀 크기가 1.45μm인 에펠 탑을 3D 현미경 스케일 객체로 인쇄하는데 성공함.

- 열-수축 방법은 구성된 격자의 photonic band-structures에 의해 색상이 나타나는 3D 물체를 인쇄하기 위한 3D TPL 시스템 (3D TPL system)의 해상도 한계를 극복할 수 있는 방법임.

- 이러한 결과는 복잡한 3D 물체 내에서 원하는 대로 구조적 색상을 생성하는 능력을 입증하였으며, 가시 광선에서 작동하는 소형 광학 부품 및 집적화 된 3D 광 회로 (integrated 3D photonic circuitry)의 개발로 확장 될 수 있음을 제시함.

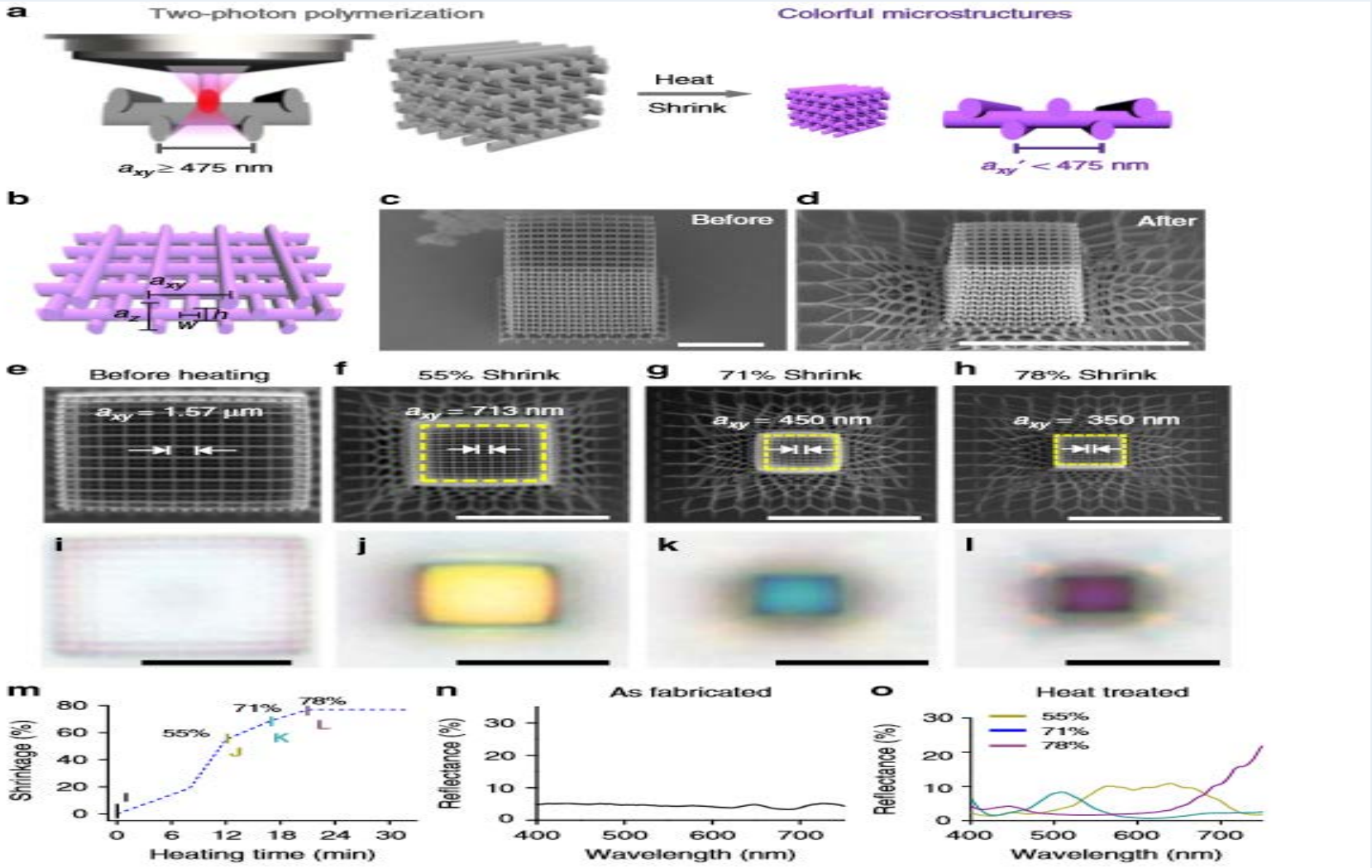

Fig. 1 Heat shrinking induced colors of 3D-printed woodpile photonic crystals. **a** Schematic of the fabrication process. Left: woodpile photonic crystal written in commercial IP-Dip resist by two-photon polymerization at dimensions well above the resolution limit of the printer to prevent structures from collapsing. Right: after heat treatment, the dimensions of the photonic crystal are reduced below the resolution limit of the printer, and colors are generated. The colors change with different degrees of shrinkage. **b** Schematic showing one axial unit of the woodpile structure. a_{xy} and a_z denote the lateral and axial lattice constants, respectively. Tilted-view scanning electron micrographs (SEM) of a representative woodpile photonic crystal (**c**) before and (**d**) after heating. SEM images and corresponding brightfield reflection-mode optical micrographs of the woodpile photonic crystal before heating (**e**, **i**) and with shrinkages of 55% (**f**, **j**), 71% (**g**, **k**), and 78% (**h**, **l**). **m** Shrinkage of the woodpile photonic crystal heated at ~450 °C as a function of heating duration. Reflectance spectra of the woodpile photonic crystal **n** before heating and **o** after heating with 55%, 71%, and 78% shrinkage. Scale bars represent 10 µm

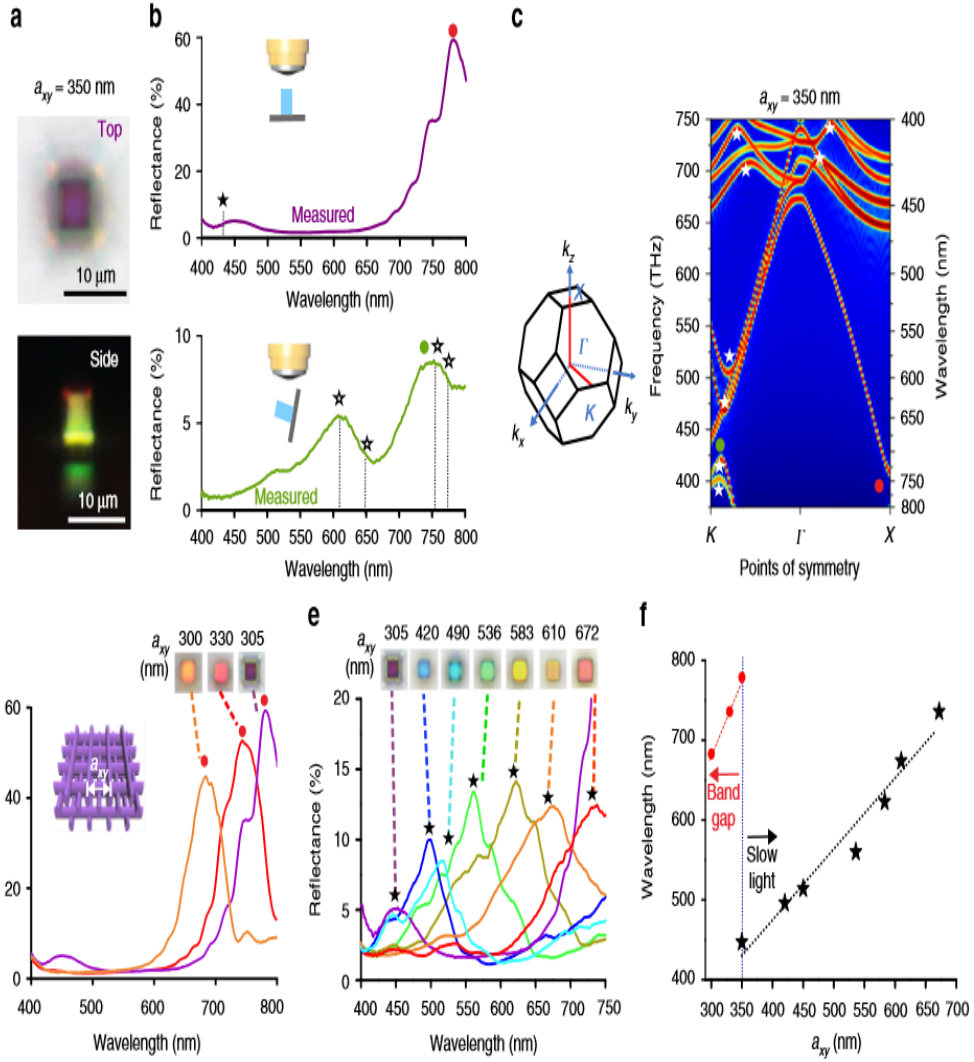

Fig. 2 Reflectance and bandstructure of a woodpile photonic crystal with $a_{xy} = 350$ nm, $a_z = 614$ nm. **a** Top view (top) and side view (bottom) reflection-mode optical micrographs of the woodpile photonic crystal. **b** Reflectance of the woodpile photonic crystal measured with top-down illumination (top) and side illumination (bottom). **c** First Brillouin zone and photonic bandstructure of the woodpile photonic crystal in the Γ-K and Γ-X directions. Stars indicate slow light modes and dots indicate stopbands. **d**, **e** Reflectance spectra and reflection-mode micrographs of woodpiles under top-down illumination conditions for $a_{xy} = 300$-350 nm (**d**) and $a_{xy} = 350$-672 nm (**e**), respectively. **f** Plot of reflectance-peak positions as a function of the lattice constant

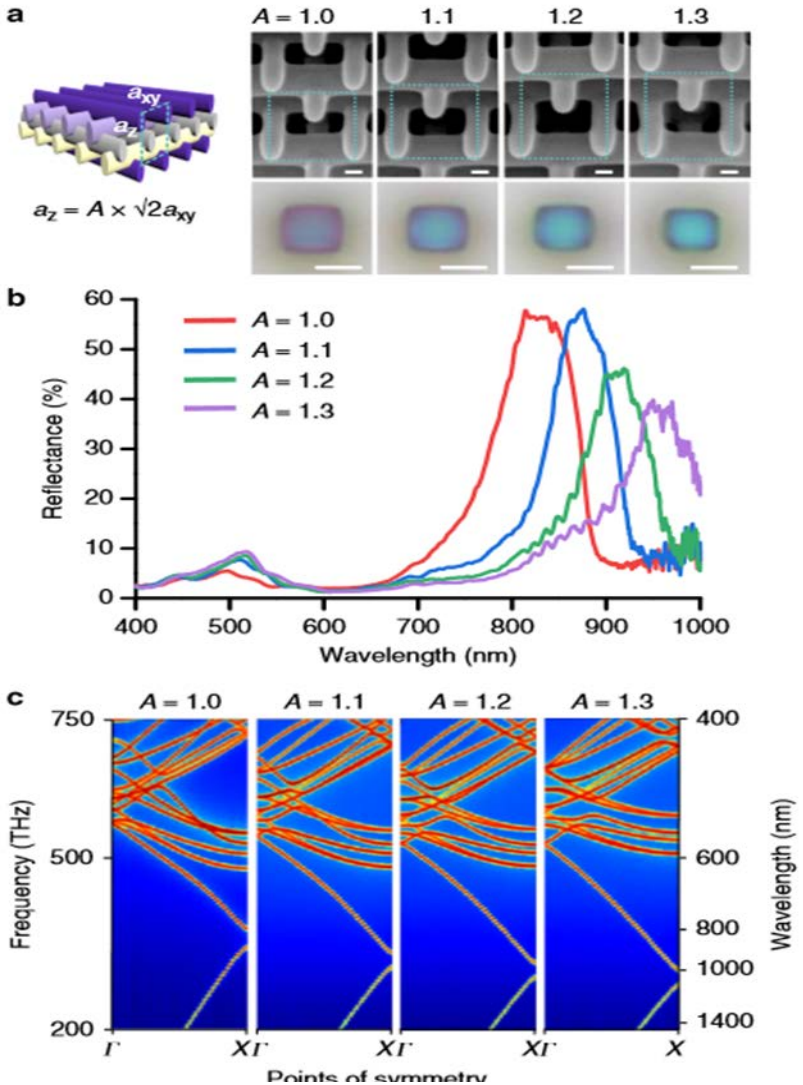

Fig. 3 Reflectances and bandstructures of woodpile structures with fixed $a_{xy} = 450$ nm and varying A, the scaling factor of a_z. **a** 45°-tilted-view SEM and reflection-mode micrographs of the woodpile photonic crystals with A varying from 1.0 to 1.3. SEM scale bars represent 100 nm and micrograph scale bars represent 5 μm. **b** Top-down reflectance spectra of the woodpile photonic crystals. **c** Bandstructures in the Γ-X direction for $A = 1.0$-1.3

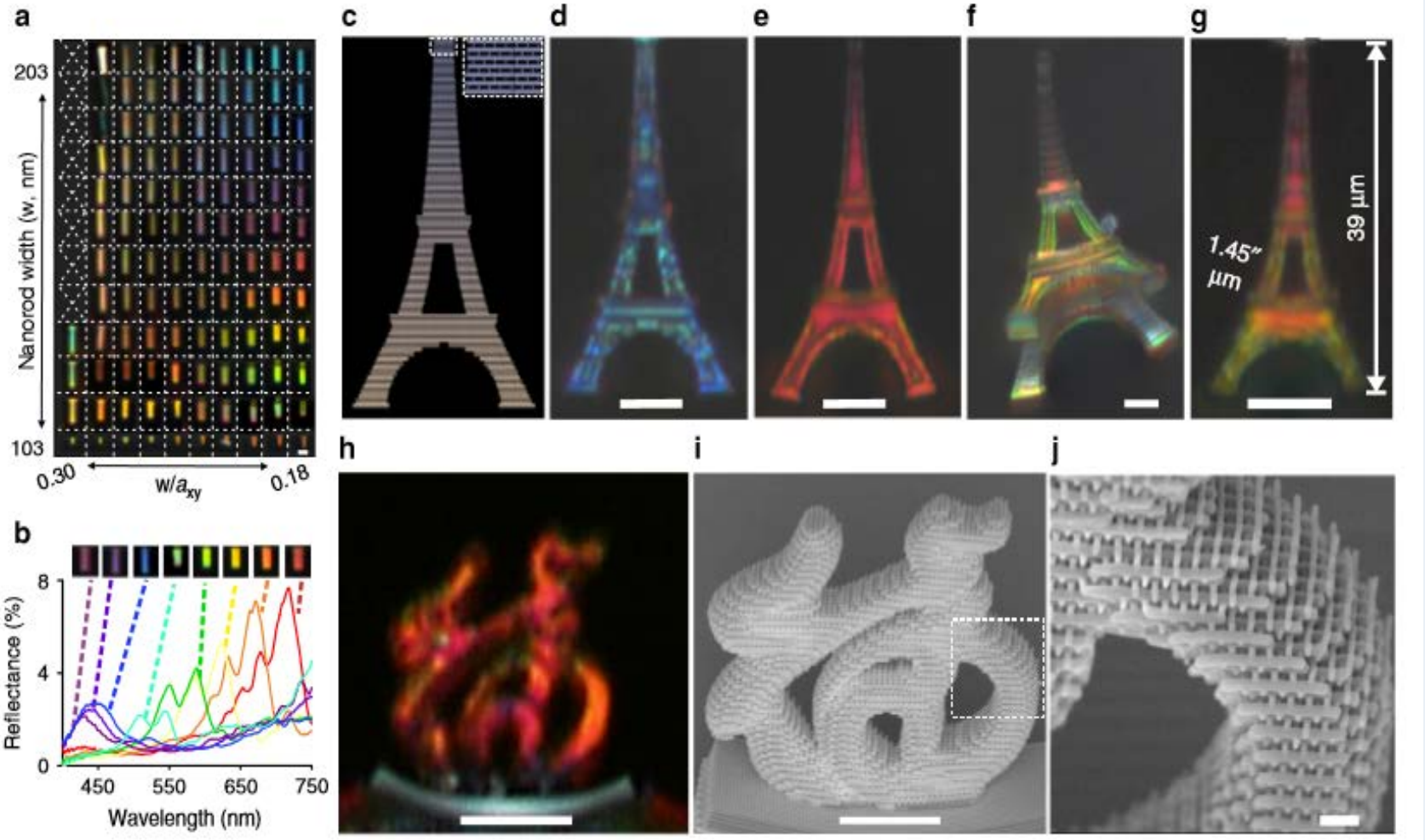

Fig. 4 3D color prints. **a** Composite optical micrographs of heat-treated woodpile photonic crystals with varying structural dimensions as viewed from the side. **b** Side illumination reflectance spectra of selected woodpile structures from **a**. **c** General Writing Language file used for lithographic printing of the Eiffel Tower, comprising of woodpile voxels. Micrographs of 3D-printed model of the Eiffel Tower in structural blue (**d**) and structural red (**e**). **f** Oblique view of an Eiffel Tower printed with intentional gradient of colors. **g** Further down-scaled multi-color 3D print of the Eiffel Tower. **h** Optical micrograph and **i** SEM image of a 3D Chinese character "福" in structural red. **j** Close-up SEM image of dotted square region in **i**. Scale bars in **a**–**i** represent 10 µm and scale bar in **j** represents 1 µm

✓ Photonic crystal for graphene plasmons[5]

- 광 결정은 주기적으로 변화하는 광학 특성을 갖는 매체에서 구현되며 집적 광 회로에서 광 전파의 제어를 가능하게 함. 물리적 개념을 모방하나 일반적인 광 결정은 작동 중 온/오프 제어에 적합하지 않음.

- 이 논문은 이러한 한계를 극복하기 위하여 표면 플라즈몬 폴라리톤 (surface plasmon polaritons)으로부터 광범위하게 조정 가능한 2 차원 광 결정을 개발함.

- 개발된 플랫폼은 나노 구조의 게이트 절연체가 있는 백 게이트 플랫폼에 집적화된 그래핀 단층으로 구성되었음. 적외선 나노-이미징은 광 게이트 갭의 형성, 인가된 게이트 전압에 의한 온/오프, 점차적으로 튜닝될 수 있는 국부 플라즈몬 밀도 상태의 강한 변조를 입증하였으며 1차원 플라즈몬 모드를 지원하는 인공 도메인 벽을 구현함.

- 정전기적으로 조정 가능한 광 결정은 표준 금속 산화물 반도체 필드 효과 트랜지스터 기술 (standard metal oxide semiconductor field effect transistor technology)에서 파생되었으며 실용적인 온 칩 조명 조작 (on-chip light manipulation)을 위한 방법을 제시함.

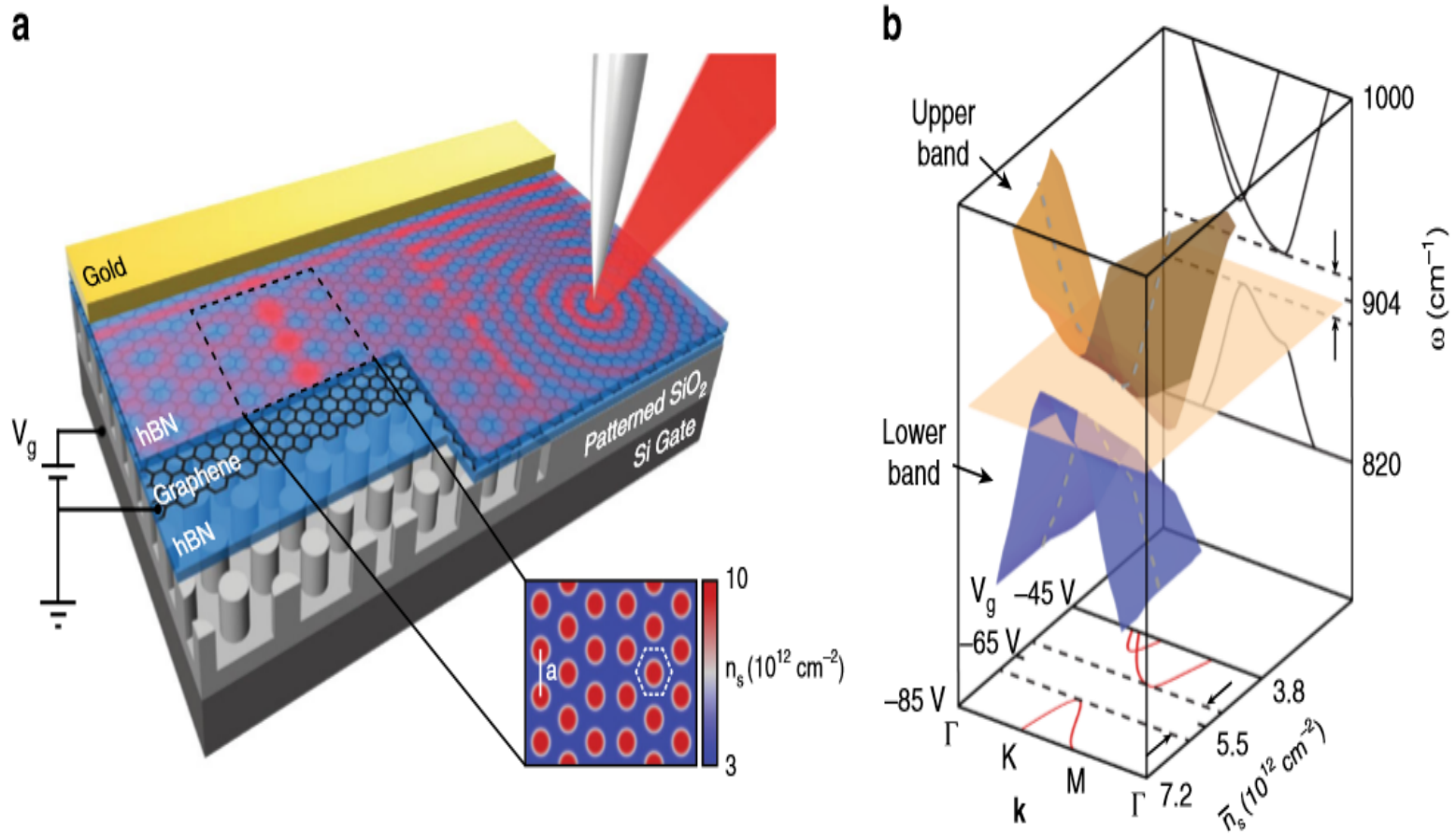

Fig. 1 Graphene photonic crystal. **a** Schematic of a photonic crystal comprised of a graphene monolayer fully-encapsulated by hexagonal boron nitride on top of an array of SiO_2 pillars. Inset, simulated carrier density map $n_s(\mathbf{r})$ at average carrier density $\bar{n}_s = 4.5\times10^{12}$ cm^{-2}, showing two hexagonal-patterned domains separated by an artificial lattice dislocation (domain wall). The lattice periodicity $a = 80$ nm. The photonic crystal unit cell is marked by a white dashed hexagon. **b** Calculated plasmonic band structure as a function of wave-vector $\mathbf{k}$ and average carrier density $\bar{n}_s$. A vertical cut parallel to the $\omega - \mathbf{k}$ plane (back panel) generates the plasmonic band structure at fixed carrier density $\bar{n}_s = 5.5\times10^{12}$ cm^{-2}. The dashed lines mark the range of a complete plasmonic bandgap. A horizontal cut parallel to $\bar{n}_s - \mathbf{k}$ plane (bottom panel) generates the plasmonic dispersion as a function of average carrier density $\bar{n}_s$ and wave-vector $\mathbf{k}$, at laser frequency $\omega = 904$ cm^{-1}; a complete bandgap is evident for carrier density around $\bar{n}_s = 5.5\times10^{12}$ cm^{-2}

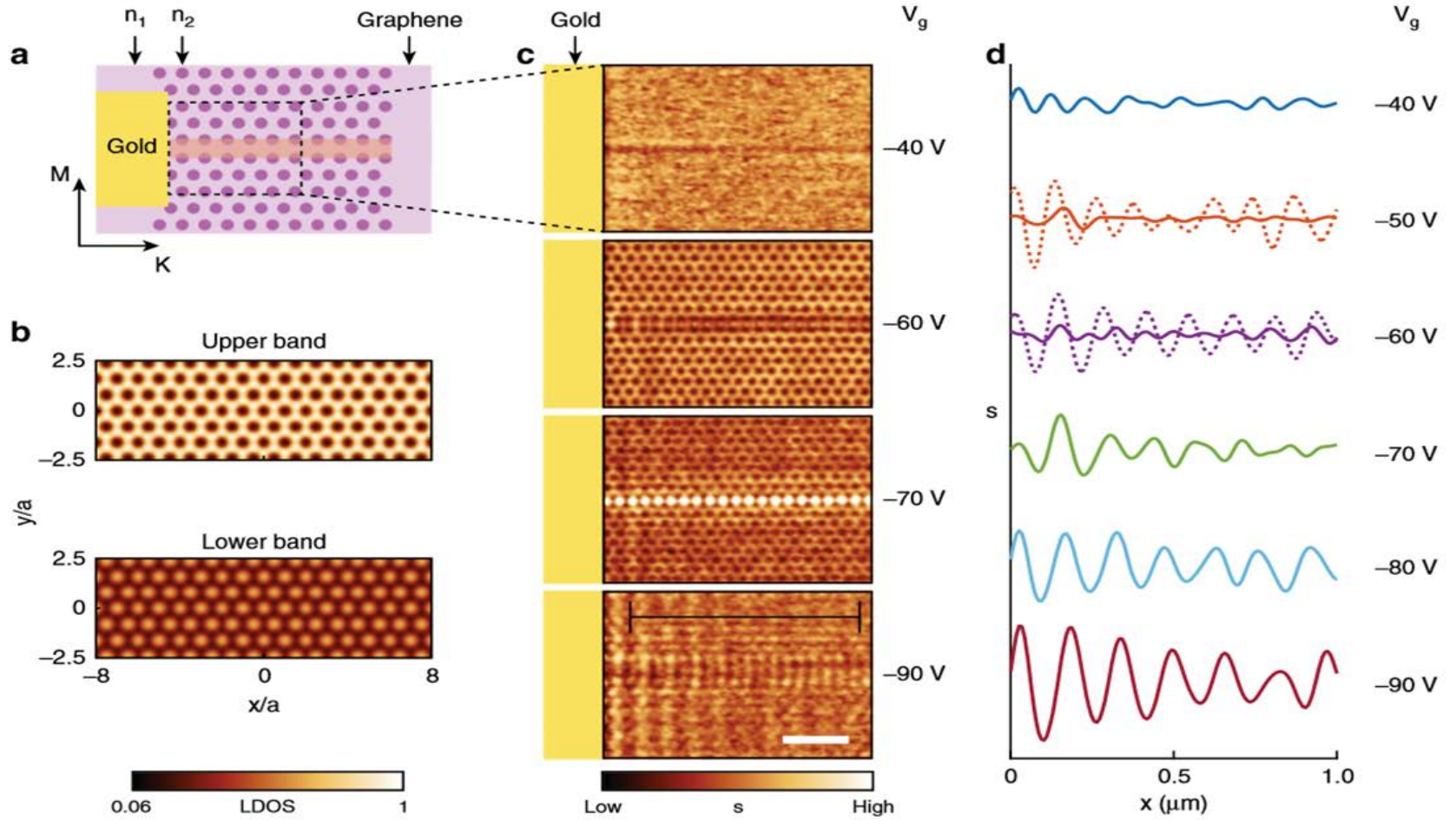

Fig. 2 Gate-tunable plasmonic response of a graphene-based photonic crystal. **a** Schematic of the photonic crystal structure with an engineered domain wall in the middle, highlighted in orange. Color contrast represents carrier density modulation $n_{1,2}$ in graphene. A gold antenna in the left serves as a plasmon launcher. The scanned area in panel **c** is marked with a dashed box. K/M directions in BZ are marked with arrows. **b** Simulated LDOS maps for upper and lower plasmonic bands. **c** Experimental near-field images $s(\mathbf{r},\omega)$ acquired at different gate voltages at $T = 60$ K and laser frequency $\omega = 904\ \mathrm{cm}^{-1}$. At $V_g = -40$ V, only faint plasmonic fringes are observed. At $V_g = -60$ V, a hexagonal pattern of dark spots emerges. At $V_g = -70$ V, a 1D domain wall state appears in the middle of the image. At $V_g = -90$ V, propagating plasmons are launched by the gold antenna on the left. This latter image also reveals a hexagonal pattern of bright spots. Black solid line marks the location of the line profiles in panel **d**. Scale bar: 400 nm. **d** Line profiles $s(\mathbf{r},\omega)$ taken in the photonic crystal region away from the domain wall. Dotted lines display the corresponding line profiles in un-patterned region. The systematic increase of SPP wavelength λ_p with carrier density n_s matches the expected scaling: $\lambda_p \propto \frac{v_F\sqrt{n_s}}{e\omega^2}$

참고 문헌

1. Bio-inspired photonic crystals for naked eye quantification of nucleic acids, K. Zhu, J. Chi, D. Zhang, B. Ma, X. Dong, J. Yang, C. Zhao* and H. Liu,* The Analyst, 144(18), 2019

2. Biomimetic Chiral Photonic Crystals, J. Lv, D. Ding, X. Yang, K. Hou, X. Miao, D. Wang, B. Kou, L. Huang and Z. Tang, Angew .Chem. 131, 2019

3. Biomimetic photonics, S. V. Boriskina , V. Greanya and K. Weir, J. Opt. 21, 2019

4. Structural color three-dimensional printing by shrinking photonic crystals, Y. Liu, H. Wang, J. Ho, R. C. Ng, R. J. H. Ng, V. H. Hall-Chen, E. H. H. Koay, Z. Dong, H. Li, C.-W. Qiu, J. R. Greer and J. K. W. Yang*, NATURE COMMUNICATIONS, 10, 2019

5. Photonic crystal for graphene plasmons, L. Xiong, C. Forsythe, M. Jung, A. S. McLeod, S. S. Sunku, Y. M. Shao, G. X. Ni, A. J. Sternbach, S. Liu, J. H. Edgar, E. J. Mele, M. M. Fogler, G. Shvets, C. R. Dean and D. N. Basov*, NATURE COMMUNICATIONS, 10, 2019